Disposable Fluidic Devices of Bionanochannels for Enzymatic Monitoring and Energy Harvesting

Tukhar Jyoti Konch, Akash Protim Bora, and Kalyan Raidongia*

Department of Chemistry, Indian Institute of Technology Guwahati, Guwahati, 781039, Assam, India

S Supporting Information

ABSTRACT: Nature produces a plethora of nanochannels to carry out highly complex biological tasks in a sophisticated manner. There have been several studies to understand the characteristics of these channels; however, efforts to apply them for technological advancements are still scarce. Here, we have demonstrated that the fluidic channels of biomaterials can be harvested as nanofluidic devices to produce energy from enzymatic chemical reactions. The bionanochannel-based nanofluidic devices exhibit various nanofluidic phenomena like surface-charged-governed ionic conductivity and development of the transmembrane potential. The mobility of ions in the hydrated bionanochannels are found to be higher than that of bulk water. The cation-selective nature of the biochannels was also exploited to harvest a continuous supply of power up to 74 mW m^{-2} for 3 h from the enzymatic decomposition of urea. The transmembrane potential across the biochannels was also explored for label-free electrical monitoring of the enzymatic reaction inside the biological medium. Electrical monitoring on the kinetics of urease at different reaction temperatures suggested that inside biological medium the reaction goes through a pathway of lower activation energy (31.1 kJ) than that in the bulk environment (34.1 kJ). Enzyme urease was found to be more sustainable in bionanochannels than in glass vials.

KEYWORDS: bionanochannels, nanofluidic ion-transport, ionic mobility, energy harvesting, enzyme kinetics
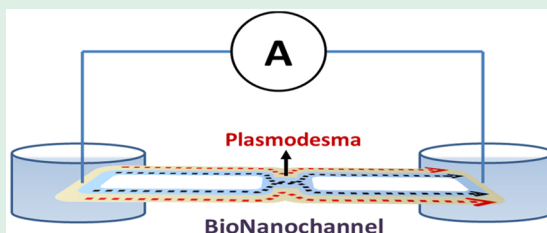
INTRODUCTION

While artificial devices and machineries are providing countless conveniences to modern life, their disposals are creating major havoc in the environment.[1] Therefore, in recent years, numerous research efforts are being dedicated to replace unsustainable materials and devices with environmentally benign alternatives of similar functionalities. For example, different kind of electronic devices such as solar cells, diagnostic tools, sensors, electrochromic displays, and artificial tissues, etc.[2−6] have been developed based on sustainable materials obtained from the environment. Similarly, the outstanding new properties of liquids confined inside nanometer sized containers promise numerous technological breakthroughs in the areas of water treatment, energy harvesting, and molecular sieving.[7−10] Studies on confined liquid also open up an avenue to understand the activity of biological nanochannels creating a platform to exploit them for various biomedical and chemical applications.[11,12] However, in practice, the excellent properties of numerous biological channels readily available to us have not been explored yet for the technological applications.

Solanum tuberosum or potato, taken here as a model system, is one of the most widely used staple foods across the globe. It exhibits very interesting internal features in the micro and nanometer regime just like any other biological system.[13,14] It also possesses a highly active fluidic network across the cell walls to facilitate communications and transport of materials between the plant cells.[15] The transport pathways of plants are divided into two types, the "living symplastic pathway" and the "dead apoplastic pathway".[16] In the symplastic pathway, movement of masses from one cell to another cell occurs through the plasmodesmata, the narrow channels that act as an intercellular cytoplasmic gate between the cells. While in the active or regulated transport, plasmodesmata dilates to accommodate much larger macromolecules or viruses through a set of highly specific and complex molecular interactions; in the passive mode, it possesses a size exclusion limit of ∼1 kDa (2−3 nm^2).[17] In the apoplastic pathway, the mass is transported through the narrow interfibrillar and intermicellar space of the cell walls and channels formed between the adjacent cell units[18−20] (Figure 1a). Carpita et al. and Marchner et al. demonstrated that the nature of molecular/ionic transport through the narrow (3−5 nm) channels of the cell walls are not free or bulk-like, and it is strongly influenced by the interactions with the nondiffusible anions of the cell wall, like the carboxyl groups of the galacturonic acids of pectin.[21,22] Motivated by the interesting nanofluidic properties of biological nanochannels, tremendous research efforts have been devoted to prepare artificial nanochannels involving various expensive and sophisticated instrumentation. However, the abundant nanofluidic channels ubiquitous in the biological systems around us have not been considered yet for
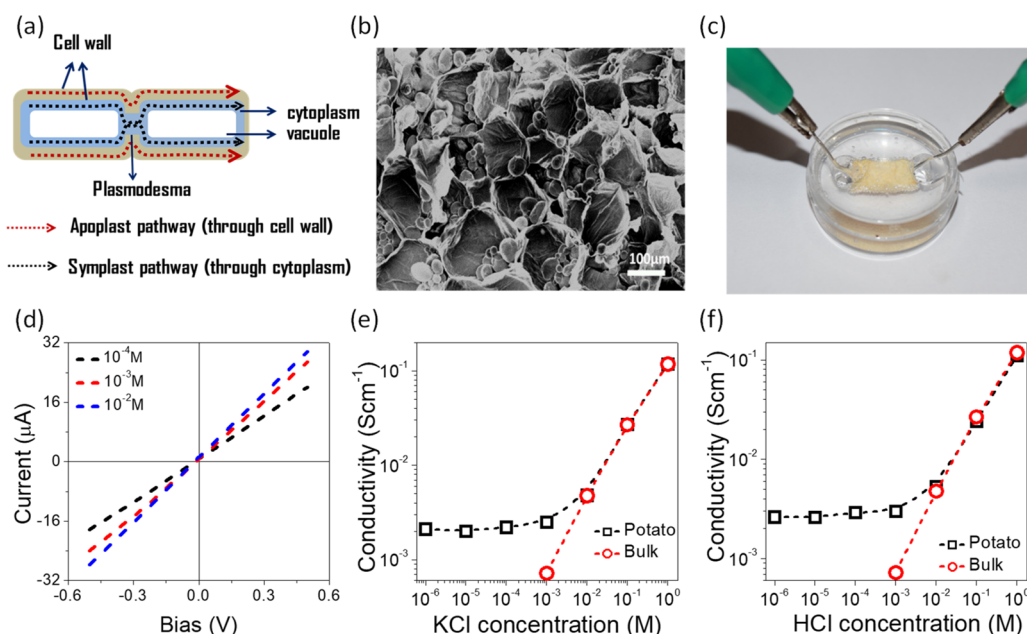
Figure 1. (a) Schematic illustration of the ion transportation pathways in the plant cell. (b) FESEM image of the cross-section, (c) digital image of the nanofluidic device, and (d) *I*−*V* curves recorded through bionanochannels of *Solanum tuberosum*. The ionic conductivities of the bionanofluidic device with different concentrations of (e) KCl and (f) HCl.

technological applications. Here, as a proof of the concept, the intracellular transport pathways of raw potato are harvested as biodegradable nanofluidic devices to produce energy from enzyme-catalyzed chemical reactions. The potato derived nanofluidic channels are also exploited to study the kinetics of enzymatic reaction inside the biological medium.

■ RESULTS AND DISCUSSION

In order to harvest nanofluidic channels of the biological system, rectangular pieces of raw potato were first dipped into liquid nitrogen, which was followed by sublimation of the frozen solvents under ultrahigh vacuum in a lypholizer instrument. After 24 h of lypholization, potato pieces were examined under electron microscopes and preserved in a desiccator until further use. A field emission scanning electron microscopic (FESEM) image of the cross-section of freeze-dried potato is shown in Figure 1b. The three major components of potato tissues, viz., cortex, storage parenchyma, and pith, are composed of tightly packed isodiametric cells, and hence under electron microscope it appears as a network of tightly packed polygonal cells. The tiny oval shaped structures (∼3−50 μm) seen in the parenchyma cellular compartments are the starch granules, the most important energy reservoir of the plants[23] (Figure 1b).

Nanofluidic devices of biochannels were fabricated by immersing freeze-dried pieces of potato (dimensions ∼20 × 4 × 0.5 mm^3) in a freshly prepared polydimethylsiloxane (PDMS) elastomer solution. After curing the elastomer at 60 °C, two reservoirs of about 0.6 mL in volume were carved out to expose both the ends of the potato strips to electrolyte solutions (Figure 1c). The as-prepared nanofluidic devices were then soaked in deionized water for 1 day to ensure complete rehydration of the biochannels. After hydration, the reservoirs were filled with electrolyte solutions of known concentrations and allowed for 6 h to reach the equilibrium. The ionic current through the biochannels were measured through Ag/AgCl electrodes inserted into the reservoirs by

employing a Keithley 2450 source meter instrument. Figure 1d shows the *I*−*V* curves recorded through a potato device with different concentrations of KCl. The linearity in the *I*−*V* curve confirms the presence of a continuous network of hydrated channels throughout the potato tuber. The ionic conductivity of the nanofluidic device was calculated by normalizing the slope of the *I*−*V* curves with the overall dimensions of the potato strip, that is length (*l*), width (*w*), and thickness (*t*) of the rectangular pieces used for the device fabrication. In Figure 1e, conductivity values calculated for the potato strip are compared with that of bulk solutions as a function of salt concentration, *I*−*V* curves recorded for bulk with different concentrations of KCl as shown in Figure S1 (Supporting Information). As typical artificial nanofluidic devices, bio-channels of the potato strip also show the characteristics of surface-charged-governed ionic conductivity. At the high concentration regime (10^{-2} M to 1 M), the conductivity values increase linearly with that of the salt concentration, but at the low concentration regime (10^{-3} M to 10^{-6} M) it did not change even for orders of magnitude change in the salt concentration. On the contrary, in the bulk water, conductivity decreases linearly with decreasing salt concentration. Such drastic different behavior of water molecules inside the biological system from that of bulk water was also predicted by Sahu et al. and Esch et al.[24,25] The walls of plant cells are made up of various polymeric materials with negative surface charges, such as celluloses, hemicelluloses, pectins, and phenolics. These negative surface charges create an electrical double layer by attracting the co-ions and repelling the counterions. When Debye lengths of the channel surfaces overlap, the concentration of ions inside the channels is determined by the surface charge density of the surrounding walls, not by the concentration of the reservoirs, leading to the surface-charge-governed ionic conductivity.[26,27] The existence of surface-charge-governed ionic conductivity not only confirmed successful construction of the biochannel-based nanofluidic devices but also indicated absence of large
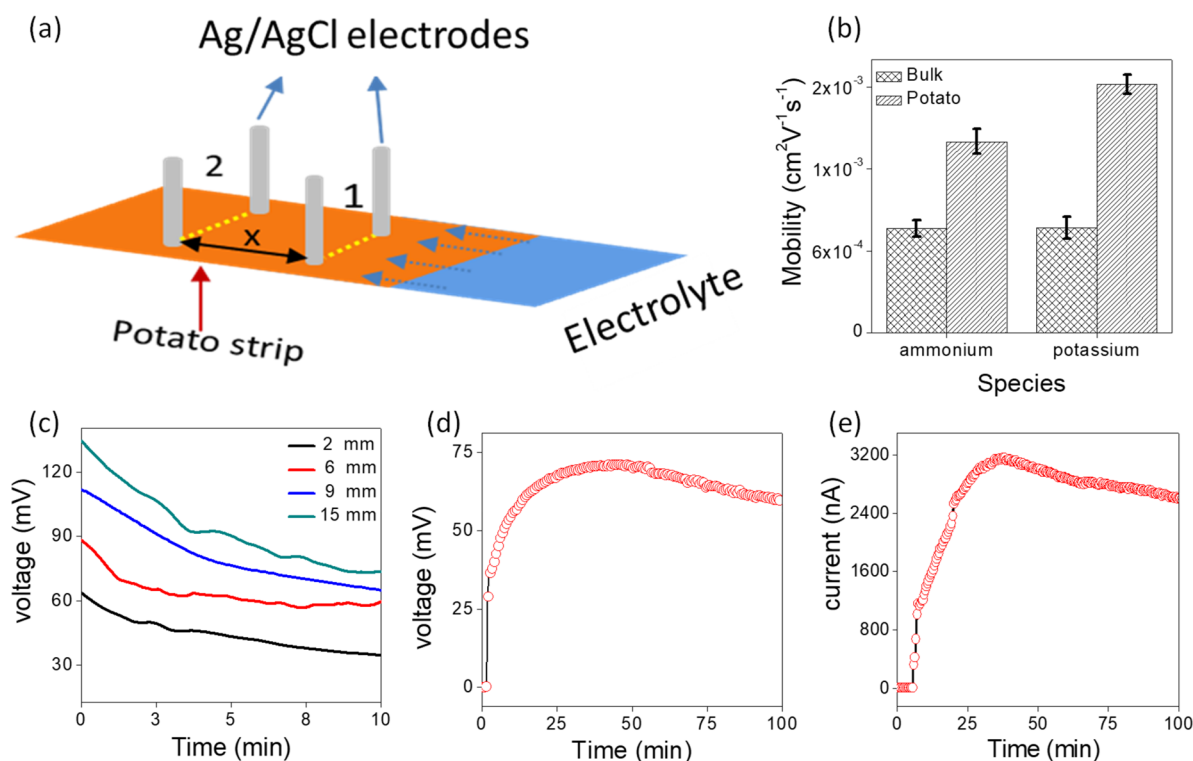
Figure 2. (a) Schematic diagram of the experimental setup used for the diffusivity measurement, (b) mobility values of different ions inside bionanochannels compared with that of bulk water, (c) transmembrane potential harvested from the concentration gradient across the potato membranes of different thickness as a function of time, and (d) transmembrane potential and (e) open circuit ionic current across the potato membrane developed by the enzymatic decomposition of urea by urease.

interconnected macropores inside the freeze-dried potato. In order to further confirm, the proton conductivity of biochannels was also measured as a function of time. As shown in Figure 1f, for the protons, the bionanofluidic device also displayed the characteristic surface-charge-governed ionic conductivity.

The fluidic network of the potato tuber contains a range of nanochannels of different sizes and shapes with specific functionalities; however, in the bioderived nanofluidic devices it is important to know the combined effective dimension (h_{eff}) of the nanochannels. The h_{eff} of the potato tuber was determined from the transition point (C_t) of conductivity vs concentration plot, the point at which the characteristics of ionic current changes from the bulk-like regime to the surface-charge-governed regime, shown in the Figure S2 (Supporting Information). From the relationship between surface charge density (σ_s) and C_t of nanofluidic channels, shown in eq 1 (Mathematical Equation section), the h_{eff} of the potato nanochannels were calculated to be 6 nm.[28,29] The rehydration characteristics of the freeze-dried potato tuber were studied by monitoring the emergence of the ionic current in the otherwise insulating ion channels. As shown in Figure 2a, liquid water was introduced to a rectangular strip of freeze-dried potato embedded in PDMS from one side and allowed to diffuse toward the other end. The ionic current was measured at two different points (near and far ends) of the potato strip to determine the rate of diffusion. At the beginning, no current was observed at either end; however, as soon as the liquid water diffused through the strip, it hydrated the ion channels displaying a sharp rise in the current values. In Figure S3a (Supporting Information), ionic current measured at the near and far ends is plotted as a function of time, and the time

difference between the saturation points at either end of the potato strip is taken as the time required for water molecules to travel the distance. The diffusivity (D) of water through the freeze-dried strip was calculated to be 1.58×10^{-6} cm^2 s^{-1}, from the time (t) taken by water molecules to travel the distance (x) between the near and far ends by using Einstein's approximation for three-dimensional diffusion[31] (eq 2). The same method was also employed to determine the diffusivity of K$^+$ and NH$_4^+$ ions by allowing 0.1 M aqueous solutions of KCl and NH$_4$Cl to diffuse from one end of the rehydrated potato tuber to the other end. The ionic current values recorded at the near and far ends for KCl and NH$_4$Cl solutions are shown in Figure S3b,c (Supporting Information), respectively. The diffusivity values of K$^+$ and NH$_4^+$ ions calculated as such were used for calculating the mobility of the ions through the potato nanochannels by employing the Nernst–Einstein equation[32] (eq 3, Figure S3d, Supporting Information). Remarkably, the mobility values of K$^+$ and NH$_4^+$ ions calculated as such are found to be higher than that in the bulk liquid as shown in the bar diagrams of Figure 2b.

The large number of ion selective channels readily available in the freeze-dried potato could have multiple applications. As a proof of concept, the same has been employed to harvest green energy from the concentration difference. A device comprised of two compartments separated by a potato tuber membrane (dimension 12.5 mm^2 × 2 mm) was fabricated by using PDMS elastomer as shown in Figure S4 (Supporting Information). The high concentration compartments (C_H) were filled with KCl solutions of 1 M concentration and the low concentration (C_L) chamber was filled with 10^{-3} M KCl solution. The trans-membrane potentials originating from the selective transport of the cations through the potato

membranes were measured by inserting two Ag/AgCl electrodes into the reservoirs. The black curve in Figure 2c shows the trans-membrane potential originating from the 3-fold concentration gradient across a potato membrane (2 mm thickness) for 10 min. The transmembrane potential develops as such declines quickly and became almost negligible after 50 min (see Figure S5 in the Supporting Information), which suggest that the potato membrane could not hold the concentration gradient for a long time. Therefore, the thickness of the membranes was successively increased from 2 mm to 15 mm, and a concomitant improvement in both the open circuit voltage was observed. However, in order to get a constant voltage supply for a longer duration, it will be ideal to have a system that constantly produces ions in an environmentally friendly manner. For the proof of concept, a nickel-dependent metalloenzyme (urease), synthesized by plants, bacteria, and fungi, is used for the constant supply of ions. When urease decomposes the substrate (urea), it produces ionic products like OH^-, HCO_3^-, and NH_4^+, which increases the conductivity of the reaction medium. It offers a convenient electrical monitoring of the enzymatic reaction. In Figure S6, the ionic conductivity of reaction medium was compared with the amount of NH_4^+ ions released from the reaction by employing the Nessler method.[33] The inherent cation selectivity of the potato membrane preferentially allows transport of the cations (NH_4^+) generated in the enzymatic reaction, creating a potential gradient across the membrane.[9] In typical experiments, both of the reservoirs were initially filled with a buffer solution (0.01 mM KCl, 1 mg/mL urease, pH 7) and held for 4 h to ensure complete rehydration of the biochannel membranes with a thickness of 2 mm. After attaining the equilibrium, 0.1 M urea was added to one of the reservoirs to carry out the enzymatic decomposition reaction. As the enzymatic reaction started producing the ions, both the open circuit potential and current started rising and reached saturation after 50 min, see Figure 2d,e. The power densities obtained from the KCl-based concentration gradient experiment and enzymatic decomposition reaction were calculated based on eq 4. Although the magnitude of the transmembrane potential (130 mV) for the KCl concentration gradient experiment was higher at the initial stage, the magnitude of the ionic current (120 nA) obtained was low (Figure S7). As a result, the maximum power density achieved from a 15 mm thickness potato membrane from the KCl concentration gradient experiment was calculated to be only ∼6 mW m^{-2}. On the other hand, the power density calculated for the enzymatic experiment following the same method was found to be 74 mW m^{-2}.

As the enzyme catalyzed reactions are crucial for the functioning of numerous biological systems, much research effort has been devoted to unveil its characteristics, both in the *in vitro* and *in vivo* conditions. While *in vivo* studies are extremely challenging, *in vitro* studies offer the convenience of applying various analytical tools to obtain detailed information about the samples. Unfortunately, the *in vitro* studies do not reflect the actual activities of enzymes inside the confinement of complex biological mediums, which motivated the researchers to synthetically imitate the molecularly crowded environment inside the channels of nanofluidic devices.[34,35] These artificial channels allow one to study activities of enzymes under confinement, but it is still far from mimicking the actual conditions of the biological environment. The nanofluidic devices of the potato offer label-free electrical

detection of enzymatic reactions under the confinement of biological nanochannels. The straightforward utilization of biological channels not only avoided the discrepancies frequently encountered in developing biomimicking artificial devices but also provided a physiological environment which is otherwise difficult to conserve in artificial units. Here, the transmembrane potential developed by the preferential migration of NH_4^+ ions was employed to monitor the characteristics of the enzymatic reactions inside the biological medium. Multiple potato strips embedded inside the PDMS elastomer were soaked with a desired aqueous solution of urea (10 mM, 8 mM, 5 mM, and 1 mM) for 6 h to make sure there was complete rehydration of the channels. After rehydration, 0.5 mL of an aqueous solution of urease (1 mg/mL) was injected into each potato strip (3 mm away from the reservoir 1), as shown in the schematic in Figure 3a. Here, one side of
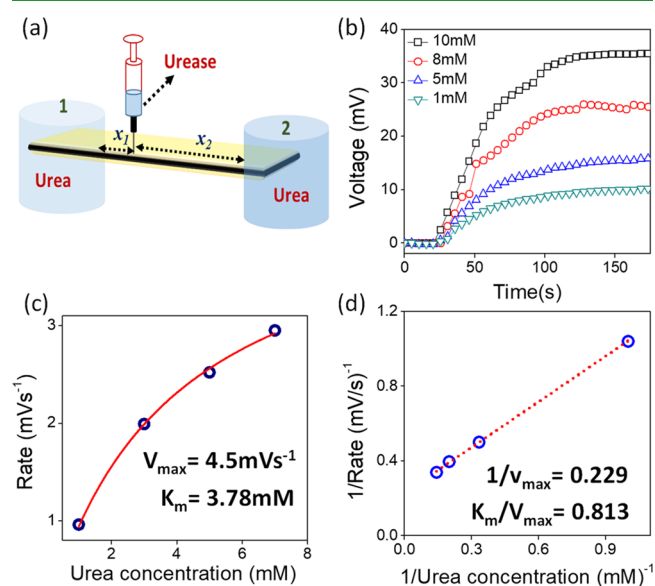
Figure 3. (a) Schematic illustration of the bionanofluidic device utilized for the study of enzyme kinetics inside bionanochannels, (b) open circuit voltage generated from the enzymatic reaction of urease starting with different substrate (urea) concentration, (c) Michaelis–Menten plot of initial reaction rate versus substrate concentration, and (d) Lineweaver–Burk double reciprocal plot of initial reaction rate vs substrate concentration. The linearization of the plot signifies the enzymatic reaction to be of first-order kinetics with respect to the substrate concentration.

the bionanofluidic system acts as an enzymatic reaction chamber and the other part as the ion-selective membrane. The membrane potentials developed as such are shown as a function of time in Figure 3b. Here, the rate of the potential development at different substrate (urea) concentrations can also be considered as the rate of ionic product formation. The initial reaction velocity (V_{int}) that is the mass of the product formed per unit time during the initial stage of the reaction was found to be proportional to the value of the membrane potential.[36] The V_{int} values for urease-catalyzed decomposition of urea for different starting concentrations of substrate (urea) were obtained by the linear fit of the curves shown in Figure 3b. The experiment was repeated several times under identical conditions, and representative results of the repetitions are shown in Figure S8. The V_{int} values obtained as such are plotted as a function of urea concentration in Figure 3c, which
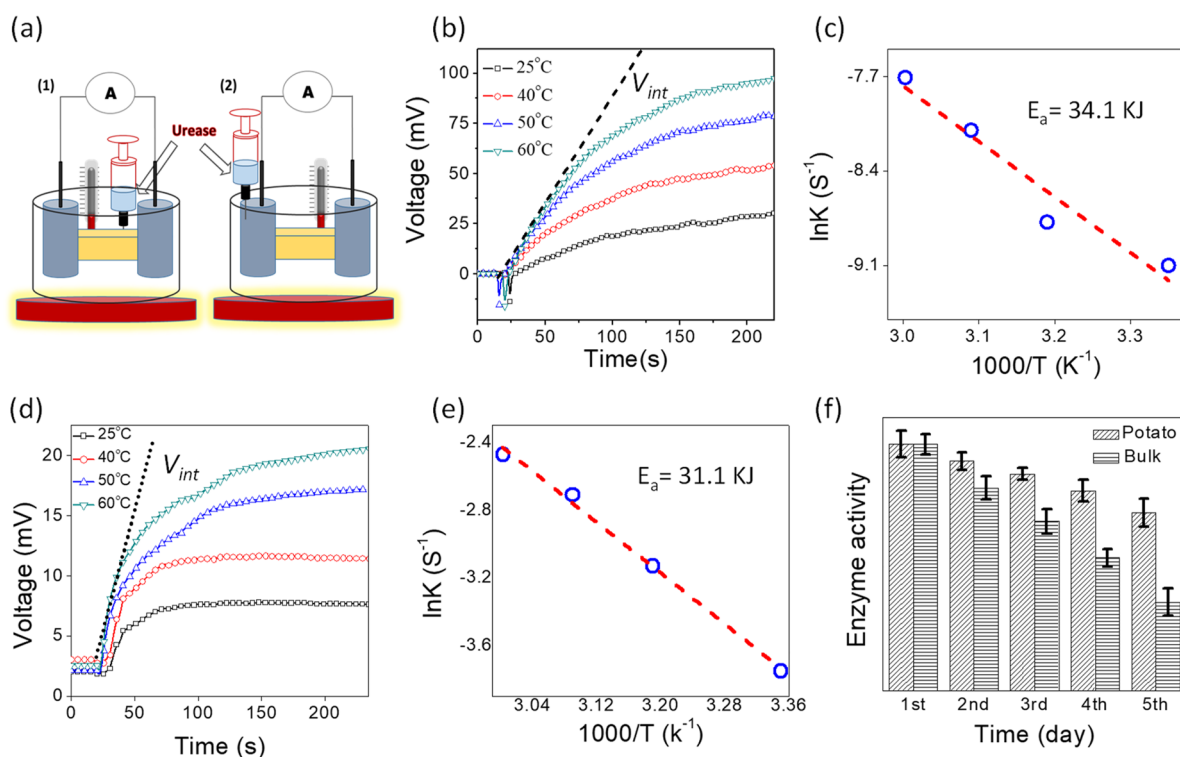
Figure 4. (a) Schematic illustration of the experimental setup used for the comparative study of enzyme kinetics. Open circuit membrane potentials developed as a function of time (b) inside versus (d) outside biochannels at the different reaction temperatures. Arrhenius plot of the rate constants for enzymatic reaction (c) inside, and (e) outside biochannels, respectively. (f) Comparison of the activity of urease inside and outside the biochannels as a function of time.

follows the Michaelis–Menten equation (eq 5).[37] From the data shown in Figure 3c, the maximum reaction velocity (V_{max}) and Michaelis–Menten constant (K_m) were found to be 4.5 mV s^{-1} and 3.78 mM, respectively. Similarly, a double reciprocal Lineweaver–Burk plot (Figure 3d, eq 6) of the initial enzymatic reaction rate vs concentration of urea was found to be linear, confirming the reaction to be of first order with respect to the substrate concentration.[36] From the linearization method, V_{max} and K_m values were calculated to be 4.36 mV s^{-1} and 3.54 mM, respectively, which are found to be in good agreement with the values obtained from the Michaelis–Menten method.

The transmembrane potential was also exploited to study the effect of reaction temperature on the enzyme kinetics. Here, the trans-membrane potential developed by the preferential migration of NH$_4^+$ ions was employed to study enzyme kinetics at different temperatures. For the temperature-dependent studies, devices were prepared by encapsulating a thermometer along with a potato strip into a freshly prepared PDMS elastomer and cured at 60 °C. The specific temperature of the reaction was maintained by placing the devices on a hot plate, and the temperature was monitored by the thermometer inserted just next to the potato channels. After soaking these devices with 10^{-2} M urea solution, 0.5 mL of urease (1 mg/mL) was injected to one end of the potato strip (schematic in Figure 4a1) and the development of open circuit membrane potentials as a function of time was monitored with a source meter instrument. Figure 4b shows the potential developed as a function of time at different reaction temperatures (see Figure S9 for the representative results of the repetitive experiments), and from the slope of the linear segments of the curves, the initial rates of the urea–urease reaction was

determined. As the enzymatic reaction follows first order kinetics with respect to the substrate (urea) concentration, the rate constant values (k_{30}, k_{40}, k_{50}, and k_{60}) at different temperatures were obtained by employing eq 7. From the Arrhenius plot of the rate constants as shown in Figure 4c, the activation energy of the reactions was found to be 31.1 kJ. For comparison purposes, the activation energy of the enzymatic reaction was also evaluated in the bulk condition. Here, instead of injecting directly into the potato strip, urease solutions were added to one of the reservoirs as shown in the schematic in Figure 4a2. The potentials developed under such conditions are plotted as a function of time at different reaction temperatures and shown in Figure 4d (results corresponding to representative repetitions of this experiment are shown in Figure S10). From the Arrhenius plot of the rate constants, the activation energy of the reactions (Figure 4e) in the bulk condition was found to 34.1 kJ, which is in good agreement with the values reported earlier in the literature.[38]

Similarly, the sustainability of urease inside the potato channels was compared with that of the bulk environment. Multiple strips of freeze-dried potatoes of similar dimensions (7 × 4 × 1 mm^3) were soaked with identical amounts of urease solutions (300 μL and 1 mg/mL) and stored in a hydrated environment. In order to monitor the activity of urease as a function of time, after every 24 h 1 mL of urea (0.01 M) was injected to one of the urease soaked potato strips, and the amount of NH$_4^+$ ions released from the reaction was determined by employing the Nessler reagent. Simultaneously, several glass vials containing 300 μL of 1 mg/mL urease solutions were stored separately, and activity of the same was determined by the same method and compared with the samples stored in the biological channels. As shown in the bar

diagrams of Figure 4f, the activity of urease was found to be declining in the glass vials at a much faster rate than that inside the biochannels, suggesting the latter to be a better medium for the enzyme activity. Similar observations about superior activity and specificity of enzymes in the biological medium are already reported in the literature.[39−44] Based on the existing knowledge, the enhancement of the activity of urease inside the potato nanochannels is attributed to the conducive biological environment, like compartmentalization of enzymes by the cells. Compartmentalization enhances the efficiency of enzymes metabolic pathways by not only maintaining a high local concentration but also providing favorable spatial and temporal organization of molecules within the cell. These complexes allow optimized substrate channelling and thereby prevent loss of intermediates and improve control and efficiency of catalysis.[40−42]

■ CONCLUSIONS

In conclusion, we have demonstrated the possibilities of employing large number of biochannels readily available in our surroundings for the technological advancements in multiple directions. The nanofluidic channels harvested from the potato tuber exhibit surface-charge-governed ionic transport and cross membrane potentials just like artificially fabricated nanofluidic membranes. As expected, inside bionanofluidic channels, cations such as K^+ and NH_4^+ exhibit mobility values higher than that of bulk water. The ion-selective nature of biochannels was also exploited for energy harvesting from concentration differences and enzymatic chemical reactions. It also provided a platform for convenient electrical monitoring of enzyme kinetics inside biological systems. The studies of the kinetics of enzymatic decomposition of urea by urease at different reaction temperatures revealed that inside biological mediums, the reaction goes through a pathway of lower activation energy than that in the bulk environment. Similarly, inside the biochannels, the activity of urease was found to be active for a longer duration of time than that in the glass vials. Finally, looking at the large variety of nanofluidic channels designed by nature to carry out highly complex biological tasks in a very sophisticated manner, it should be possible to design/develop different kinds of nanofluidic devices for future applications.

■ EXPERIMENTAL SECTION

Materials. Urease, potassium chloride, and Nessler reagent were purchased from Sigma-Aldrich. Urea and hydrochloric acid were purchased from Merck. Ammonium chloride was purchased from Rankem. Polydimethylsiloxane (PDMS) was purchased from Sylgard.

Characterization. The potato samples were lyophilized with the help of a Labconco Freezone 4.5 L-50C Benchtop freeze-dryer. The morphology of the potato samples was characterized by a field emission scanning electron microscope (FESEM) (Zeiss, model Sigma). All the electrochemical measurements were performed with the help of a source meter (Keithley 2450 model). The concentration of the colored complex HgO·(HgNH₂)I was determined by using a UV−vis spectrophotometer (Systronics, UV−vis spectrophotometer 117).

Methods. *Surface Charge Governed Ionic Transport.* Nanofluidic devices of potato biochannels were fabricated by embedding strips of the freeze-dried potato tubers of known dimensions in the PDMS elastomer. The ends of the strips were exposed to electrolyte solutions by carving out reservoirs on the PDMS stub at either end of the strip. Ag/AgCl electrodes which are connected to the terminals of a Keithley source meter (model 2450) were immersed in the reservoirs filled with electrolytes at both ends of the strip. Representative I−V curves for the potato strips were recorded at

different electrolyte concentrations ranging from 10^{-6} M to 1 M by sweeping voltage from −0.5 V to 0.5 across each strip. Conductivity calculations were done using the following equation:

$$C = G \times \text{cell constant}$$

where C is the conductivity, and G is the conductance.

Enzyme Sustainability Measurement. Multiple strips of freeze-dried potatoes of similar dimensions were soaked with identical amounts of urease solutions (300 μL, 1 mg/mL) and stored in a hydrated environment. After every 24 h, 1 mL of urea was injected into one of the urease soaked potato strips. Enzymatic decomposition of urea releases ammonium ions, which was sensed by introducing a dilute solution of Nessler reagent. The initially colorless solution of ammonium ion turns light yellow upon addition of the Nessler reagent. The concentration of ammonium ion produced during the enzymatic decomposition was quantified from the absorbance values of Millon's base HgO·Hg(NH₂)I by UV−vis spectroscopy. Simultaneously, several glass vials containing 300 μL of 1 mg/mL urease solutions were stored separately, and activity of the same was determined by the same method and compared with the samples stored in the biological channels.

Mathematical Equations. Effective nanochannel height calculation:

$$h = \frac{10^{-3}\sigma_s}{eN_A c_t} \tag{1}$$

where N_A and e stands for Avogadro's number and elementary charge, respectively. The σ_s value of the cell wall (-2.3 mC m^{-2}) was determined by Obi et al. by employing the electrophoresis method based on the Gouy−Champman−Stern model.[30]

Einstein diffusivity equation:

$$x^2 = 6Dt \tag{2}$$

where x is the distance between the two electrodes mounted between the near and far ends, t is the time required for the electrolyte to travel the distance x, and D is the diffusivity.

Nernst−Einstein equation:

$$\mu = \frac{eD}{kT} \tag{3}$$

where k is the Boltzmann constant and T is the absolute temperature.

Power density calculation:

$$\text{power density} = \frac{V_{max} \times I_{max}}{\text{area}} \tag{4}$$

where V_{max} and I_{max} represent the maximum stable voltage and current, respectively.

Michaelis−Menten equation:

$$V = \frac{V_{max}[S]}{K_m + [S]} \tag{5}$$

where V_{max} represents the maximum velocity achieved by the system, [S] is the substrate concentration, and K_m is the Michaelis constant.

Lineweaver−Burk equation:

$$\frac{1}{V} = \frac{K_m}{V_{max}}\frac{1}{[S]} + \frac{1}{V_{max}} \tag{6}$$

First order enzymatic rate equation:

$$V = K[S] \tag{7}$$

where V represents the rate of the reaction, [S] is the concentration of the substrate, and K is the rate constant.

■ ASSOCIATED CONTENT

ⓢ Supporting Information

The Supporting Information is available free of charge on the ACS Publications website at DOI: 10.1021/acsabm.9b00249.

$I-V$ curves recorded for bulk KCl of different concentrations, transition point determination from conductance vs concentration plot, current response plot of diffusivity measurement, schematic diagram of the concentration gradient-based energy harvesting device, long-time operability of concentration gradient-based open circuit voltage generation experiment, calibration curves of enzyme kinetics, open circuit current harvested from concentration gradient-based experiment, and ammonium ion concentration determination from UV−vis spectroscopy (PDF)

■ AUTHOR INFORMATION

Corresponding Author

*E-mail: k.raidongia@iitg.ernet.in.

ORCID ⊙

Kalyan Raidongia: 0000-0001-7829-7498

Notes

The authors declare no competing financial interest.

■ ACKNOWLEDGMENTS

■ REFERENCES

(1) Irimia-Vladu. Green" Electronics: Biodegradable and Biocompatible Materials and Devices for Sustainable Future. *Chem. Soc. Rev.* **2014**, *43*, 588−610.

(2) Cheng, Q.; Ye, D.; Yang, W.; Zhang, S.; Chen, H.; Chang, C.; Zhang, L. Construction of Transparent Cellulose-Based Nanocomposite Papers and Potential Application in Flexible Solar Cells. *ACS Sustainable Chem. Eng.* **2018**, *6*, 8040−8047.

(3) Kim, Y. J.; Wu, W.; Chun, S.-E.; Whitacre, J. F.; Bettinger, C. J. Biologically Derived Melanin Electrodes in Aqueous Sodium-Ion Energy Storage Devices. *Proc. Natl. Acad. Sci. U. S. A.* **2013**, *110*, 20912−20917.

(4) Yin, L.; Cheng, H.; Mao, S.; Haasch, R.; Liu, Y.; Xie, X.; Hwang, S.-W.; Jain, H.; Kang, S.-K.; Su, Y.; Li, R.; Huang, Y.; Rogers, J. A. Dissolvable Metals for Transient Electronics. *Adv. Funct. Mater.* **2014**, *24*, 645−658.

(5) Rullyani, C.; Sung, C.-F.; Lin, H.-C.; Chu, C.-W. Flexible Organic Thin Film Transistors Incorporating a Biodegradable CO_2-Based Polymer as the Substrate and Dielectric Material. *Sci. Rep.* **2018**, *8*, 8146.

(6) Song, M.; Cheng, M.; Xiao, M.; Zhang, L.; Ju, G.; Shi, F. Biomimicking of a Swim Bladder and Its Application as a Mini-Generator. *Adv. Mater.* **2017**, *29*, 1603312.

(7) Li, W.; Wu, W.; Li, Z. Controlling Interlayer Spacing of Graphene Oxide Membranes by External Pressure Regulation. *ACS Nano* **2018**, *12*, 9309−9317.

(8) Ji, J.; Kang, Q.; Zhou, Y.; Feng, Y.; Chen, X.; Yuan, J.; Guo, W.; Wei, Y.; Jiang, L. Osmotic Power Generation with Positively and Negatively Charged 2D Nanofluidic Membrane Pairs. *Adv. Funct. Mater.* **2017**, *27*, 1603623.

(9) Lin, L.; Zhang, L.; Wang, L.; Li, J. Energy Harvesting from Enzymatic Biowaste Reaction through Polyelectrolyte Functionalized 2D Nanofluidic Channels. *Chem. Sci.* **2016**, *7*, 3645−3648.

(10) Li, H.; Song, Z.; Zhang, X.; Huang, Y.; Li, S.; Mao, Y.; Ploehn, H. J.; Bao, Y.; Yu, M. Ultrathin, Molecular-Sieving Graphene Oxide Membranes for Selective Hydrogen Separation. *Science* **2013**, *342*, 95−98.

(11) de la Escosura-Muniz, A.; Merkoci, A. Nanochannels Preparation and Application in Biosensing. *ACS Nano* **2012**, *6*, 7556−7583.

(12) Li, R.; Fan, X.; Liu, Z.; Zhai, J. Smart Bioinspired Nanochannels and their Applications in Energy-Conversion Systems. *Adv. Mater.* **2017**, *29*, 1702983.

(13) Vaananen, T.; Ikonen, T.; Rokka, V.-M.; Kuronen, P.; Serimaa, R.; Ollilainen, V. Influence of Incorporated Wild Solanum Genomes on PotatoProperties in Terms of Starch Nanostructure and GlycoalkaloidContent. *J. Agric. Food Chem.* **2005**, *53*, 5313−5325.

(14) Konstankiewicz, K.; Czachor, H.; Gancarz, M.; Król, A.; Pawlak, K.; Zdunek, A. Cell Structural Parameters of Potato Tuber Tissue. *Int. Agrophys.* **2002**, *16*, 119−127.

(15) Sattelmacher, B. The Apoplast and Its Significance for Plant Mineral Nutrition. *New Phytol.* **2001**, *149*, 167−192.

(16) Münch, E. *Die Stoffbewegung in Der Pflanze*; Gustav Fischer: Jena, Germany, 1930.

(17) Lee, J.-Y.; Lu, H. Plasmodesmata: the Battleground against Intruders. *Trends Plant Sci.* **2011**, *16*, 201−210.

(18) Gogarten, J. P. Physical Properties of the Cell wall of Photoautotrophic Suspension Cells from Chenopodium Rubrum L. *Planta* **1988**, *174*, 333−339.

(19) Chesson, A.; Gardner, P. T.; Wood, T. J. Cell Wall Porosity and Available Surface Area of Wheat Straw and Wheat Grain Fractions. *J. Sci. Food Agric.* **1997**, *75*, 289−295.

(20) Moon, R. J.; Martini, A.; Nairn, J.; Simonsen, J.; Youngblood, J. Cellulose Nanomaterials Review: structure, Properties and Nanocomposites. *Chem. Soc. Rev.* **2011**, *40*, 3941−3994.

(21) Carpita, N.; Sabularse, D.; Montezinos, D.; Delmer, D. Determination of the Pore Size of Cell Walls of Living Plant Cells. *Science* **1979**, *205*, 1144−1147.

(22) Marschner, H. *Mineral Nutrition of Higher Plants*; Academic Press: San Diego, CA, 1995.

(23) Smith, A. M. The Biosynthesis of Starch Granules. *Biomacromolecules* **2001**, *2*, 335−341.

(24) Sahu, K.; Mondal, S. K.; Ghosh, S.; Bhattacharyya, K. Ultrafast Dynamics in Biological Systems and in Nano-Confined Environments. *Bull. Chem. Soc. Jpn.* **2007**, *80*, 1033−1043.

(25) Esch, M.; Sukhorukov, V. L.; Kurschner, M.; Zimmermann, U. Dielectric properties of Alginate Beads and Bound Water Relaxation Studied by Electrorotation. *Biopolymers* **1999**, *50*, 227−237.

(26) Wang, C.; Wang, S.; Chen, G.; Kong, W.; Ping, W.; Dai, J.; Pastel, G.; Xie, H.; He, S.; Das, S.; Hu, L. Flexible, Bio-Compatible Nanofluidic Ion Conductor. *Chem. Mater.* **2018**, *30*, 7707−7713.

(27) Raidongia, K.; Huang, J. Nanofluidic Ion Transport through Reconstructed Layered Materials. *J. Am. Chem. Soc.* **2012**, *134*, 16528−16531.

(28) Schoch, R. B.; Renaud, P. Ion Transport through Nanoslits Dominated by the Effective Surface Charge. *Appl. Phys. Lett.* **2005**, *86*, 253111.

(29) Konch, T. J.; Gogoi, R. K.; Gogoi, A.; Saha, K.; Deka, J.; Reddy, K. A.; Raidongia, K. Nanofluidic Transport through Humic Acid Modified Graphene Oxide Nanochannels. *Mater. Chem. Front.* **2018**, *2*, 1647−1654.

(30) Obi, I.; Kakutani, T.; Imaizumi, N.; Ichikawa, Y.; Senda, M. Surface Charge Density of Hetero-Fused Plant Protoplasts: an Electrophoretic Study. *Plant Cell Physiol.* **1990**, *31*, 1031−1037.

(31) Einstein, A. Über die von der Molekularkinetischen Theorie der Wärme Geforderte Bewegung von in Ruhenden Flüssigkeiten Suspendierten Teilchen. *Ann. Phys. (Berlin, Ger.)* **1905**, *322*, 549−560.

(32) Marsh, R. A.; Waight, S. G.; Wycombe, H. The Effect of pH on the Zeta Potentialof Wheat and Potato Starch. *Starch* **1982**, *34*, 149−152.

(33) Jeong, H.; Park, J.; Kim, H. Determination of NH_4^+ in Environmental Water with Interfering Substances Using the Modified Nessler Method. *J. Chem.* **2013**, *2013*, 359217.

(34) Küchler, A.; Yoshimoto, M.; Luginbühl, S.; Mavelli, F.; Walde, P. Enzymatic Reactions in Confined Environments. *Nat. Nanotechnol.* **2016**, *11*, 409−420.

(35) Durand, N. F. Y.; Renaud, P. Label-free Determination of Protein-Surface Interaction Kinetics by Ionic Conductance inside a Nanochannel. *Lab Chip* **2009**, *9*, 319−324.

(36) Orosco, M. M.; Pacholski, C.; Sailor, M. J. Real-time Monitoring of Enzyme Activity in a Mesoporous Silicon Double Layer. *Nat. Nanotechnol.* **2009**, *4*, 255−258.

(37) Casali, L.; Mazzei, L.; Shemchuk, O.; Honer, K.; Grepioni, F.; Ciurli, S.; Braga, D.; Baltrusaitis, J. Smart Urea Ionic Co-crystals with Enhanced Urease Inhibition Activity for Improved Nitrogen Cycle Management. *Chem. Commun.* **2018**, *54*, 7637−7640.

(38) Fidaleo, M.; Lavecchia, R. Kinetic Study of Enzymatic Urea Hydrolysis in the pH Range 4−9. *Chem. Biochem. Eng. Q.* **2003**, *17*, 311−318.

(39) Wang, H.; Zhao, Z.; Liu, Y.; Shao, C.; Bian, F.; Zhao, Y. Biomimetic Enzyme Cascade Reaction System in Microfluidic Electrospray Microcapsules. *Sci. Adv.* **2018**, *4*, No. eaat2816.

(40) Conrado, R. J.; Varner, J. D.; DeLisa, M. P. Engineering the Spatial Organization of Metabolic Enzymes: Mimicking Nature's Synergy. *Curr. Opin. Biotechnol.* **2008**, *19*, 492−499.

(41) Zhao, Z.; Fu, J.; Dhakal, S.; Johnson-Buck, A.; Liu, M.; Zhang, T.; Woodbury, N. W.; Liu, Y.; Walter, N. G.; Yan, H. Nanocaged Enzymes with Enhanced Catalytic Activity and Increased Stability Against Protease Digestion. *Nat. Commun.* **2016**, *7*, 10619.

(42) Küchler, A.; Yoshimoto, M.; Luginbühl, S.; Mavelli, F.; Walde, P. Enzymatic reactions in confined environments. *Nat. Nanotechnol.* **2016**, *11*, 409−420.

(43) Ge, J.; Lei, J.; Zare, R. N. Protein-inorganic hybrid nanoflowers. *Nat. Nanotechnol.* **2012**, *7*, 428−432.

(44) Yan, M.; Ge, J.; Liu, Z.; Ouyang, P. Encapsulation of Single Enzyme in Nanogel with Enhanced Biocatalytic Activity and Stability. *J. Am. Chem. Soc.* **2006**, *128*, 11008−11009.